Pb isotope evidence for rapid accretion and differentiation of planetary embryos

Connelly, J. N.; Schiller, M.; Bizzarro, M.

Published in:
Earth and Planetary Science Letters

DOI:
10.1016/j.epsl.2019.115722

Publication date:
2019

Document version
Publisher's PDF, also known as Version of record

Earth and Planetary Science Letters 525 (2019) 115722

Contents lists available at ScienceDirect

Earth and Planetary Science Letters

www.elsevier.com/locate/epsl

Pb isotope evidence for rapid accretion and differentiation of planetary embryos

J.N. Connelly *, M. Schiller, M. Bizzarro

Centre for Star and Planet Formation, GLOBE Institute, University of Copenhagen, Øster Voldgade 5-7, Copenhagen, 1350, Denmark

ARTICLE INFO

Article history:
Received 10 April 2019
Received in revised form 14 July 2019
Accepted 19 July 2019
Available online 13 August 2019
Editor: R. Dasgupta

Keywords:
Steinbach meteorite
Pb-Pb chronology
Al-Mg isotopes
accretion timescale
planetary embryo

ABSTRACT

Group IVA iron and siliate-iron meteorites record a large range of cooling rates attributed to an impact-related disruption of a molten and differentiated ca. 1000 km diameter planetary embryo of chondritic composition before re-accretion of mainly the metallic core with minor silicates. To better understand the timing of primary accretion, disruption, re-accretion and cooling of the Group IVA parent body, we have determined Pb-Pb and Al-Mg ages for the Group IVA silicate-iron Steinbach meteorite. A Pb-Pb age based on multiple fractions of late-phase, slowly-cooled orthopyroxene from Steinbach yields an absolute age of 4565.47 ± 0.30 Ma corresponding to a relative age of 1.83 ± 0.34 Myr after formation of calcium-aluminium-rich inclusions (CAIs). This is the oldest U-corrected Pb-Pb absolute age for a differentiated meteorite. We use the deficit Al-Mg dating method on one whole rock sample and two mineral separates to produce a model age of $1.3^{+0.5}_{-0.3}$ Myr after CAI formation corresponding to the depletion age of Al relative to Mg in the source material for Steinbach. Assuming this fractionation event occurred in the pre-impact parent body, this provides a maximum time after CAI formation for the disruption of the original Group IVA parent body. Together, these ages require that the original parent body accreted very early and differentiated prior to the impact-related break up, re-accretion and cooling between $1.3^{+0.5}_{-0.3}$ Myr and 1.83 ± 0.34 Myr after CAI formation. These ages are fully consistent with a growing body of evidence from meteorites and astronomical observation supporting the early and efficient growth of planetary embryos and with numerical models of pebble accretion that predict rapid growth of embryos in the presence of chondrules. This time frame for the efficient formation of planetary embryos by chondrule accretion is inconsistent with a proposed ~1.5 Myr delay in chondrule formation, a contradiction that is resolved by a non-canonical abundance of ^{26}Al in the inner Solar System during at least the first million years of the protoplanetary disk.

1. Introduction

The timing of earliest planetary embryo formation is an important parameter in understanding the dynamics of the evolving protoplanetary disk and final planetary architecture of the Solar System. Recent numerical models predict that planetary embryos will grow efficiently and rapidly in the presence of mm-sized precursor material (e.g. Johansen et al., 2015). As such, sizable bodies are predicted to have existed within the present resolution of our chronometers (several 100,000 years) after the first formation of chondrules, mm- to cm-sized inclusions that represent melted dust clumps and the most abundant component of primitive meteorites. In this view, the timing of the first formation of chondrules offers an upper limit on the earliest time for efficient accretion of sizable bodies within the Solar System but there is considerable debate over their formation ages. A traditional perspective is based on the decay of the short-lived ^{26}Al to ^{26}Mg and envisions a 1-2 Myr gap between the formation of the Sun and establishment of a protoplanetary disk and the onset of chondrule formation (e.g. Nagashima et al., 2018). However, short-lived chronometric systems rely on the unverified assumption of a homogeneous distribution of the parent nuclide throughout the protoplanetary disk. A more recent view based on the U-Pb decay system suggests that chondrules formed abundantly within the first Myr of the protoplanetary disk and that they were recycled throughout the lifetime of disk, lasting approximately 4 Myr (Bollard et al., 2017). Accepting the pebble accretion model as the most viable mechanism to efficiently grow planetary embryos, the existence of a 1-2 Myr gap between Solar System and chondrule formation implied by Al-Mg chronometry predicts that planetary embryos would have been delayed in their first appearance. In contrast, the Pb-Pb ages of chondrules predict that they would have formed in the earliest stages of the protoplanetary disk.

* Corresponding author.
E-mail address: connelly@snm.ku.dk (J.N. Connelly).

https://doi.org/10.1016/j.epsl.2019.115722

While further work appears necessary to reach a consensus on the ages of the oldest chondrules, avenues exist to evaluate the timing of formation of the earliest formed planetary embryos. The ^{182}Hf-^{182}W system applied to iron meteorites is capable of dating the timing of core formation of planetary embryos when accurately corrected for cosmogenic effects. A recent study of iron meteorites shows that some of their parent bodies had already formed, melted and differentiated into a mantle and core within 1.6 ± 1.0 Myr after Solar System formation (Kruijer et al., 2013). In addition, it is widely believed that melting and differentiation is driven by heat generated by the decay of ^{26}Al. Depending on the initial ^{26}Al/^{27}Al ratio in the bulk Solar System, some thermal models predict that planetary embryos must have formed within the first 500,000 years after the formation of the Solar System for there to be enough ^{26}Al radiogenic heat available for melting (e.g. Schiller et al., 2011, 2015; Larsen et al., 2016; van Kooten et al., 2016; Blackburn et al., 2017).

To contribute to the understanding of the earliest stages of planet formation, we report Pb-Pb and Al-Mg ages for the mixed silicate-metal meteorite Steinbach that has been grouped with IVA iron meteorites on the basis of compositional and textural similarities of the metal components (Schaudy et al., 1972). This class of meteorites is of particular interest given that they have been dated by the ^{182}Hf-^{182}W system (Kruijer et al., 2013) and there exists a single Pb-Pb age on IVA Muonionalusta that was reported as the oldest absolute age for a differentiated meteorite at 4565.3 ± 0.1 Ma (Blichert-Toft et al., 2010).

2. Steinbach and IVA iron meteorites

Steinbach is a silicate-iron meteorite found in Germany in 1724 with a total mass of 98 kg (Meteoritical Bulletin Database; https://www.lpi.usra.edu/meteor/). Steinbach contains mm-size silicate grains interspersed with mm- to cm-size grains of metal and troilite. The silicate portion is dominated by three types of pyroxene (combined 40%), tridymite (20-30%) and Fe-Ni metal and troilite (combined 30-40%) with minor amounts of chromite. Clinobronzite and Type 1 pyroxene (orthobronzite), as described by Ruzicka and Hutson (2006), have overlapping compositions and are both inclusion-rich. The more abundant inclusion-poor Type 2 pyroxene of Ruzicka and Hutson (2006) (orthobronzite) can be divided into two subgroups designated as depleted and enriched based on the abundances of Ca and Al and trace elements Cr, V, Sc, Ti, Y and Zr. Clinobronzite, Type 1 pyroxene and depleted Type 2 pyroxene have overlapping major element compositions that are distinct from the more evolved enriched Type 2 pyroxene that have a greater range of compositions. Based on textures and chemical compositions, clinobronzite, Type 1 pyroxene and depleted Type 2 pyroxene are inferred to have formed early during rapid cooling whereas enriched Type 2 pyroxene formed later during slow cooling (Ruzicka and Hutson, 2006).

Steinbach is paired with IVA iron meteorites based on the composition and structure of the metal portion (Schaudy et al., 1972; Reid et al., 1974). This group as a whole records an unusual and complex cooling history with an early rapid cooling phase (~100 °C/yr; Haack et al., 1996) followed by slower cooling (~100 °C/Myr; Yang et al., 2008). This cooling history is consistent with the distinct cooling paths recorded in the different pyroxenes of Steinbach. Most attempts to explain the complex cooling histories of IVA meteorites invoke an impact-related disruption of the parent body as part of its history. The more recent model of Ruzicka and Hutson (2006) appears to best account for all existing data where they invoke impact disruption of a molten or partially molten and already differentiated planetary embryo. The early rapid cooling over hours represents the crystallization prior to and during re-accretion with heat efficiently lost from smaller objects. The slow, protracted cooling phase represents post-accretion crystallization within the interior of the body.

3. Methods

3.1. U and Pb isotope analyses

From a 22 g slab of the Steinbach meteorite acquired from L. Labenne, a ~1 g piece was cut off using a diamond-coated wire saw (dry), crushed, sieved and sorted into different mineral concentrates using a Frantz™ magnetic separator. Five fractions of pure orthopyroxene (enriched Type 2 pyroxene of Ruzicka and Hutson, 2006) ranging in weight from 10 to 94 mg were hand picked using a binocular microscope from the magnetically-separated fractions with the greatest concentration of this phase. In five separate sessions, the pyroxene separates were washed with alternating cycles of distilled water, ethanol and acetone with five minutes of ultrasonication between each step. This was repeated five times. Each separate was then treated five times with 0.01 M HBr on a 100 °C hotplate for 15 min and ultrasonicated before rinsing with distilled water three times. Each fraction was then subjected to a progressive dissolution procedure using acids increasingly aggressive on silicates with acid strengths as outlined in Table 1. Each digestion step included heating on a hotplate at 120 °C for times listed in Table 1 followed by five minutes of ultrasonication.

The residual solid component of each step was allowed to settle after ultrasonication before the liquid was transferred to a clean Savillex™ PFA vial with care not to include any residual solid material. For those steps that did not include HF, 50 µl of 29 M HF was added to the solution after it was transferred. The final residues were fully dissolved in 29 M HF and 7 M HNO_3 on a hotplate at 135 °C for three days. All dissolution steps were spiked with an equal-atom ^{202}Pb-^{205}Pb tracer to correct for instrumental mass fractionation prior to the final evaporation and re-dissolution in 1 M HBr, the acid required for the start of the chemical separation procedure. After analyzing all the dissolution steps from the first session, it was realized that the relatively weak acids of the first four steps were dominated by terrestrial contaminant Pb so that the progressive dissolution procedure was modified for the four remaining aliquots (where L1 = 1 M HBr and L2 = 4 M HNO_3). For these aliquots, only the remaining three dissolution steps (L3, L4 and L5) using HCl and HF acid were analyzed in the remaining four sessions (Table 1).

A single 100 mg fraction of pure troilite was also processed for Pb isotope analysis. This fraction was rinsed in five cycles of distilled water, ethanol and acetone on the hotplate (110 °C) followed by five minutes of ultrasonication. After addition of an equal-atom ^{202}Pb-^{205}Pb tracer, the troilite was then fully dissolved in 4 M HNO_3 on a hotplate at 110 °C for 24 h.

Lead from the pyroxene partial dissolution steps and the troilite sample was purified in two passes over a 55 µl column filled with Eichrom Industries™ anion resin following the procedures of Connelly and Bizzarro (2009). After the second pass, the samples were dried down with a 10 µl of 0.1 M H_3PO_4. The samples were loaded onto outgassed zone-refined Re ribbon with silica gel made following the recipe of Gerstenberger and Haase (1997) but using four times more silicic acid than they recommended. The isotopic composition of Pb was determined using the ThermoScientific™ Triton™ thermal ionization mass spectrometer at the Centre for Star and Planet Formation (StarPlan), University of Copenhagen, Denmark. Given the low amounts of Pb present in the pyroxene dissolution steps, all analyses were made using an axially-positioned secondary electron multiplier – ion counter (SEM-IC) where each Pb isotope was measured sequentially in peak jumping

Table 1
Pb isotope data for Steinbach.

Fraction	Acid	Treatment	Pb (pg)[1]	$^{206}Pb/^{204}Pb$[2]	$^{204}Pb/^{206}Pb$[3]	Error (%)[4]	$^{207}Pb/^{206}Pb$[3]	Error (%)[4]	Rho[5]	$^{208}Pb/^{206}Pb$[3]	$^{208}Pb/^{204}Pb$[3]
Pyx1-L1	0.05 M HBr	24 h + US	311.0	18.146	0.0549468	0.0273	0.856959	0.0124	0.01	2.09958	38.2111
Pyx1-L2	0.05 M HBr	24 h + US	225.8	18.132	0.0549748	0.0350	0.857102	0.0150	0.01	2.10179	38.2318
Pyx1-L3	1 M HBr	3hr + US	56.0	18.138	0.0548909	0.0520	0.858067	0.0213	0.05	2.10425	38.3351
Pyx1-L4	0.5 M HBr	12 h + US	8.6	18.113	0.0545816	0.1008	0.854761	0.0325	0.18	2.08460	38.1924
Pyx1-R[6]	HF-HNO_3	3 days + US	32.4	22.331	0.0444220	0.0709	0.813126	0.0258	0.70	1.77915	40.0512
Pyx2-L3	6 M HCl	30 min + US	118.0	18.366	0.0543192	0.0705	0.865995	0.0310	0.00	2.08621	38.4065
Pyx2-L4	1 M HF	15 min + US	20.2	43.834	0.0221593	0.3316	0.720411	0.0446	0.99	1.07600	48.5576
Pyx2-R[6]	HF-HNO_3	3 days + US	23.0	303.080	0.0027289	2.8650	0.636226	0.0576	0.99	0.47407	173.7233
Pyx3-L3	6 M HCl	30 min + US	351.7	18.307	0.0544167	0.0313	0.854308	0.0135	0.00	2.08496	38.3147
Pyx3-L4	1 M HF	15 min + US	12.0	35.944	0.0268729	0.4292	0.737312	0.0660	0.98	1.18608	44.1367
Pyx3-R[6]	HF-HNO_3	3 days + US	9.1	145.000	0.0054864	3.7396	0.647987	0.1297	0.99	0.55723	101.5649
Pyx4-L3	6 M HCl	30 min + US	36.9	17.791	0.0558827	0.0858	0.873777	0.0272	0.19	2.11185	37.7908
Pyx4-L4[6]	1 M HF	15min + US	7.0	27.472	0.0349328	0.4681	0.772860	0.0824	0.97	1.45966	41.7849
Pyx4-R	HF-HNO_3	3 days + US	19.8	37.341	0.0261124	0.2752	0.732288	0.0422	0.98	1.16680	44.6836
Pyx5-L3	6 M HCl	30 min + US	2.4	18.154	0.0530627	0.1994	0.844463	0.0629	0.00	2.06010	38.8239
Pyx5-L4	1 M HF	15 min + US	1.7	83.774	0.0052345	24.1508	0.645906	0.6371	1.00	0.49449	94.4677
Pyx5-R[6]	HF-HNO_3	3 days + US	6.3	294.650	0.0014359	23.4384	0.630840	0.1768	1.00	0.39241	273.2919
Pyrite R[6]	4 M HNO_3	1 day + US	957706.1	18.164	0.0548872	0.0348	0.857318	0.0170	0.00	2.10494	38.3503

NOTES:
1. Total amount of Pb in each fraction corrected for spike and blank.
2. Measured isotope ratio.
3. Isotope ratio corrected for mass fractionation, spike and blank.
4. Percent uncertainty on the isotopic ratio reported at the 2-sigma level.
5. Rho value for the $^{207}Pb/^{206}Pb$ and $^{204}Pb/^{206}Pb$ ratios.
6. Fractions used in the regression to define an age for Steinbach.

mode by switching the magnetic field. The much greater abundance of Pb from the troilite allowed for a static multi-collector Faraday measurement on all masses except ^{202}Pb and ^{205}Pb, which were measured on the SEM-IC. All data was reduced using an in-house program with the final regression and age calculation using Isoplot (Ludwig, 2003).

Duplicate Pb blank analyses were run with each of the five dissolution series. These comprised adding a ^{208}Pb tracer to the same type of pre-cleaned vial that was used for the sample solutions and subjecting this blank sample to the final dry down and full chemistry. The average laboratory Pb blank for the five sessions was 0.25 ± 0.05 pg, an amount that is subtracted from each analyses assuming a modern terrestrial Pb isotopic composition after Stacey and Kramers (1975).

The U isotopic composition of this sample is required for the determination of a Pb-Pb age from the pyroxene and troilite fractions. Two separate whole rock fragments (4.85 and 18.50 g) were processed by pre-dissolving the samples in a 60 ml Savillex™ PFA jar on the hot plate for five days. The residual solid portion was transferred into a 15 ml Savillex™ vial that was placed in a Parr Instruments™ bomb in an oven at 210 °C for five days with concentrated HF and HNO_3 in 3:1 proportions. Upon cooling, the supernatant was removed to the 60 ml Savillex™ jar and the residual solid component was subjected to a second round of HF-HNO_3 in the oven at 210 °C for five days. The solution and any solids from the second round were combined with the liquid from the earlier dissolution rounds, dried down and re-dissolved in 6 M HCl. After 24 h, some solid remained so that 7 M HNO_3 was added in equal volumes with the 6 M HCl. This procedure was repeated once more after which the sample was fully in solution in 50 ml of acid. This was dried down again and re-dissolved in 7 M HNO_3, the acid required for the start of the U purification procedure.

Uranium was purified from the matrix elements in a four step procedure as outlined in Connelly et al. (2012) and Livermore et al. (2018). In short, the procedure starts with replicate passes over a column filled with 1 ml of Eichrom Industries'™ UTEVA™ followed by two separate columns filled with 0.5 ml and 0.055 ml of anion resin, also from Eichrom Industries™. According to the size of the sample, they were divided into multiple UTEVA columns for the first pass so that no more than 3.7 g of dissolved sample was loaded onto a single column. The U eluted from multiple columns in the first chemistry step was recombined and processed on single columns for the remaining three steps. The final U aliquots were dried down and re-dissolved with concentrated HCl (two days), concentrated HCl and HNO_3 (two days) and concentrated HNO_3 (one day) to break down any remaining organics from the resins. The U isotopic compositions were measured using a ThermoScientific™ Neptune Plus™ multiple collector inductively coupled plasma mass spectrometer (MC-ICP-MS) at StarPlan. Given the small amounts of U isolated from the two samples, they were run only once each bracketed by two standard analyses (CRM112a; $^{238}U/^{235}U = 137.841$ after Richter et al., 2010 and Condon et al., 2010) before and after the analyses. On peak baselines were measured before each standard and sample analyses as full analyses with all data processed offline using the data reduction software Iolite (Paton et al., 2011) that is run within the Igor Pro™ software. Background intensities were interpolated using a smoothed cubic spline function, as were changes in mass bias over the course of the run. Iolite's smooth spline auto choice was used.

3.2. Al and Mg isotope analyses

In addition to an aliquot of the whole rock dissolution for U isotope measurement, a magnetically separated and subsequently handpicked mineral separate of orthopyroxene and a non-magnetic fraction were analyzed for magnesium isotopes. After complete dissolution, Al/Mg ratios of each sample were determined with a 2% accuracy using a ThermoScientific™ X-Series II™ inductively coupled plasma source mass spectrometer (ICP-MS) located at StarPlan. Magnesium was purified by ion exchange chromatography and its isotopic composition analyzed using a ThermoScientific™ Neptune Plus™ MC-ICP-MS equipped with a Sampler Jet and Skimmer X-cone and an ESI™ Apex™ sample introduction system lo-

Table 2
U isotope data for Steinbach.

Sample	Mass (g)	U (ng)	U (ppb)	^{238}U (V)	^{238}U/^{235}U	2 SE (abs)	ε^{238}U[a]	2 SE (ε units)	n
Steinbeck WR1	4.85	1.5	0.31	1.0	137.784	0.072	−4.14	5.23	1
Steinbeck WR2	19.00	18.5	0.98	18.6	137.787	0.010	−3.92	0.73	1

[a] Offset from the standard CRM-112a in parts per 10,000 with the standard ^{238}U/^{235}U ratio = 137.841 (Richter et al., 2010; Condon et al., 2010).

cated at StarPlan, following protocols outlined in Bizzarro et al. (2011) and Schiller et al. (2015). The Mg isotope composition was measured in high-resolution mode using a 50 µm entrance slit ($M/\Delta M > 5000$). At an uptake rate of ~30 µL/min, the sensitivity of the instrument was ~100 V/ppm and samples were analyzed with a total beam intensity of ~50 V. Single analyses comprised 1667 s of data acquisition and each sample was bracketed by standard analyses and analyzed ten times. Mg isotope data are reported in the μ-notation (ppm) as relative deviations from the DTS-2b standard ($\mu^{25}Mg_{DSM\text{-}3} = -122 \pm 17$ ppm (2 SD); Bizzarro et al., 2011) according to the following formula:

$$\mu^{x}Mg = [(^{x}Mg/^{24}Mg)_{sample}/(^{x}Mg/^{24}Mg)_{DTS\text{-}2b} - 1] \times 10^{6}, \quad (1)$$

where x is either 25 or 26. The mass-independent component of ^{26}Mg (μ^{26}Mg*) represents deviations from the internally normalized ^{26}Mg/^{24}Mg of the sample from the reference standard, normalized to ^{25}Mg/^{24}Mg = 0.126896 (Bizzarro et al., 2011) using the exponential mass fractionation law. All Mg isotope data was reduced off-line using Iolite (Paton et al., 2011) and changes in mass bias with time were interpolated using a smoothed cubic spline. Individual analyses of a sample were combined to produce a weighted average by the propagated uncertainties of individual analyses and reported final uncertainties are the 2 SE of the mean.

4. Results

4.1. Uranium isotopes

For the U isotopic composition (Table 2), the first fragment of 4.85 g yielded only 1.5 ng of U with an isotopic composition of 137.784 ± 0.072 where the large uncertainties reflect the low amount of U analyzed. The second fragment of 18.5 g yielded 100 ng of U with an isotopic composition of 137.787 ± 0.010. The disproportionate amount of U in the second fragment is attributed to the inclusion of an unknown U-rich phase that must have been mostly avoided in the first fragment.

4.2. Lead isotopes

The 100 mg sample of troilite contained 0.95 µg of Pb with an isotopic composition that overlaps the range of modern terrestrial Pb (Table 1). Both the very large amount and composition of this Pb indicate that it is of terrestrial origin and that the troilite and, most probably, the sample as a whole is highly contaminated with modern terrestrial Pb. Given the antiquity of this find, the origin of this terrestrial Pb is unknown. Whatever the source, it has been greatly concentrated in the troilite, likely due to the naturally greater permeability than the single crystals of silicates, including the pyroxene that was analyzed. Adding a drop of distilled water to the surface of the slab demonstrates that the troilite readily absorbs liquid over the silicate phases.

The first dissolution series of pyroxene (Pyx1) resulted in 4 of 5 dissolution steps L1-L4) returning Pb isotope compositions that overlap modern terrestrial Pb, further indicating that this sample is highly contaminated with terrestrial Pb. The subsequent four dissolution series of pyroxene (Pyx2–Pyx5) were modified in an attempt to more aggressively remove the contaminant Pb in the early dissolution steps and yield a more radiogenic residual component. This was successful to varying degrees for the successive pyroxene fractions (Pyx2–Pyx5) with a range of Pb isotopic compositions for L3 through to the residue (R) in these fractions that lie between modern terrestrial Pb and a pure radiogenic Pb component (Table 1, Fig. 1). The regression of the troilite fraction, four of five pyroxene residues and L4 from Pyx4 yields a statistically acceptable line (MSWD = 0.2) with a y-axis intercept of 0.62474 ± 0.00012 on the inverse Pb-Pb diagram (Fig. 1). We infer this value to represent the isotopic composition of the radiogenic Pb that has accumulated in the pyroxene as a result of U decay since closure of this phase. The use of these analyses to define the radiogenic Pb composition is justified by two main arguments. First, observations and theoretical arguments predict that the latest steps in any stepwise cleaning and dissolution are most likely to reduce a three component Pb system to the two component Pb system required to define the radiogenic Pb composition (Connelly et al., 2017). Second, the small errors on individual analyses and the orientation and shape of the error ellipses on the inverse Pb-Pb diagrams make it very unlikely that statistically acceptable lines that pass through the measured modern terrestrial Pb composition can be coincidently defined by multiple residue analyses that do not represent a meaningful two-component system.

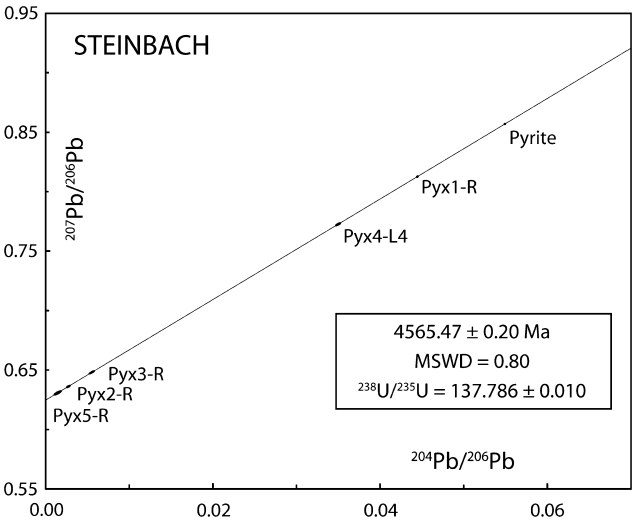

Fig. 1. Pb-Pb diagram for the silicate-iron meteorite Steinbach.

Integrated with the measured ^{238}U/^{235}U ratio of 137.787 ± 0.010, the determined radiogenic Pb composition corresponds to an age of 4565.47 ± 0.30 Ma, where the uncertainty reflects the age uncertainties related to the Pb (±0.28 Ma) and U (±0.11 Ma) isotopic analyses added in quadrature. This corresponds to a relative age of 1.83 ± 0.34 Ma after calcium-aluminium inclusion (CAI) formation at 4567.30 ± 0.16 Ma (Connelly et al., 2012), where the uncertainty reflects uncertainties on both Steinbach and the CAI ages added in quadrature.

The lack of any isotopic compositions more primitive than terrestrial Pb suggests that this sample essentially lacked initial Pb at the time of its formation. Only three of 21 Pb isotopic mea-

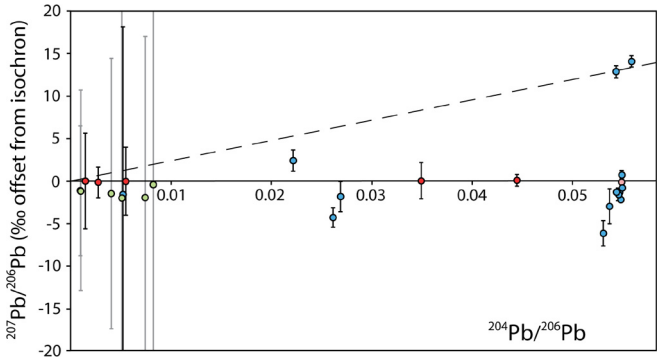

Fig. 2. Pb-Pb diagram of Fig. 1 recast so that the *x*-axis corresponds to the isochron defined by type 2 pyroxene of Ruzicka and Hutson (2006) (four residues and one L4 - red) and pyrite (pink). The rejected points from this study (blue) are shown with the data from Blichert-Toft et al. (2010) (green with grey error bars). The *y*-axis error bars show the 2-sigma ^{207}Pb/^{206}Pb errors and do not reflect the error correlation of each point. For points without error bars, the estimated uncertainties are smaller than the symbol. Dashed line projects from the radiogenic Pb composition defined by the isochron to the initial Pb isotopic composition of the Solar System after Connelly et al. (2008).

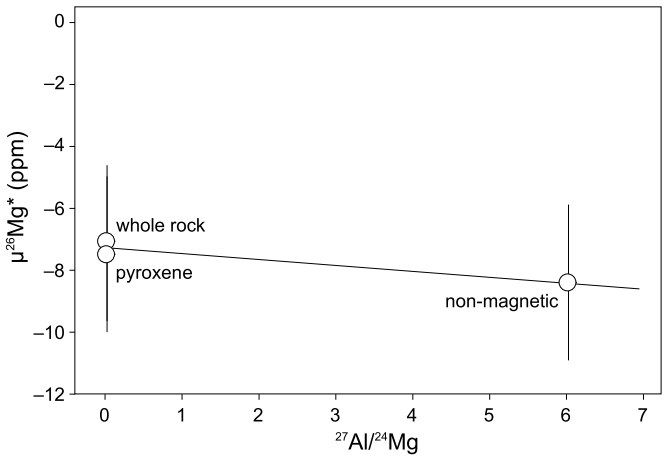

Fig. 3. ^{26}Al–^{26}Mg isochron diagram for the whole rock and mineral separates from Steinbach. Uncertainties for μ^{26}Mg* values are the 2 SE of the individual measurements, errors for the ^{27}Al/^{24}Mg analyses are smaller than the symbols. The negative regression implies a lack of resolvable radiogenic ^{26}Mg ingrowth.

surements (Pyx2-L3, Pyx2-L4 and Pyx4-L3) plot above the isochron defined by the troilite, four residues and one L4 fraction (Fig. 2). These points plot on or below a line connecting the inferred radiogenic Pb isotopic composition for this sample and the Solar System initial Pb isotopic composition, consistent with these three fractions containing a component of initial Pb (Connelly et al., 2008). That this component of Pb is present in only two of the five pyroxene separates suggests that it may not be present in the pyroxene but rather in an unidentified phase that was avoided in three of the five separates processed. Assuming all ^{204}Pb in the three fractions plotting above the array represents Solar System composition initial Pb, we calculate that the total initial Pb concentration in the five fractions analysed is 0.75 ppb. The analyses that plot below the array (Fig. 2) between Pb from troilite and radiogenic Pb are inferred to reflect various sources of contaminant Pb that are distinct from the dominant terrestrial Pb contamination recorded by the troilite and that is most robustly fixed in the pyroxene fractions. It is important to note that, while multiple sources of Pb clearly exist in the early dissolution steps, the alignment of four of five residues, one L4 aliquot and the troilite analyses is indicative of a simple two component mixture of radiogenic Pb and a single source of terrestrial contaminant Pb. This is consistent with the removal of more labile contaminant Pb and initial Pb-bearing phases in the earlier dissolution steps so that only the final or near final steps of the pyroxene fractions are reduced to a two component system.

4.3. Al-Mg systematics

One pyroxene mineral separate and one whole rock returned ^{27}Al/^{24}Mg values of 0.009 and 0.012 corresponding to μ^{26}Mg* values of -7.1 ± 2.7 and -7.5 ± 1.5, respectively. A single analysis of a non-magnetic fraction, most likely tridymite and other minor phases as inclusions, returned a ^{27}Al/^{24}Mg value of 6.02 and a μ^{26}Mg* value of -8.4 ± 2.7 (Fig. 3, Table 3). The ^{27}Al/^{24}Mg ratio of the whole rock is an order of magnitude lower than the bulk solar value of 0.1 such that radiogenic ingrowth of ^{26}Mg since cooling and closure of Steinbach must have been minimal.

5. Discussion

Our age of 4565.47 ± 0.30 Ma for the IVA paired Steinbach meteorite represents the oldest U-corrected Pb-Pb absolute age for a differentiated meteorite. Although ^{182}Hf-^{182}W age of 1.6 ± 1.0 Ma after t_0 derived from IVA iron meteorites overlaps this age (Kruijer et al., 2013), this system dates the timing of silicate-metal segregation via a model age rather than the crystallization age of a specific meteorite.

Previously published Pb-Pb results for the IVA Muonionalusta iron meteorite returned an age of 4565.1 ± 0.1 Ma (Blichert-Toft et al., 2010), an age that agrees at face value with our result. However, their reported age is problematic for several reasons. Most importantly, the calculation of the age used the previously accepted ^{238}U/^{235}U ratio of 137.88, a value that is significantly higher than any other estimates for differentiated meteorites or chondrules that have been reported in the meantime (Connelly et al., 2012; Goldmann et al., 2015; Brennecka et al., 2015; Bollard et al., 2017) and our measured value for this meteorite (Fig. 4). Assuming a solar value of 137.786 (Connelly et al., 2012) or the value we determine for Steinbach requires that this age be adjusted downward by ~1 Myr. Secondly, the uncertainty of ±0.1 Ma cannot be reproduced from their published data by the error calculation algorithm in Isoplot (Ludwig, 2003), the standard method for calculating regressions and uncertainties of isochron ages for meteoritic materials. Recalculating their tabulated data using Isoplot, assuming a ^{238}U/^{235}U ratio of 137.786 and assigning reasonable error correlations of 0.98 for such radiogenic compositions returns an age and uncertainty of 4564.1 ± 2.6 Ma. While Blichert-Toft et al. (2010) may have been motivated by sound reasoning to eliminate the transgression of error ellipses into forbidden negative space on the inverse Pb-Pb diagram, the large difference in the estimated uncertainties between the two approaches requires at least

Table 3
Al-Mg isotope data for Steinbach.

Fraction	^{27}Al/^{24}Mg	μ^{26}Mg* (ppm)	2 SE	μ^{25}Mg (ppm)$_{DTS-2b}$	2 SE	μ^{26}Mg (ppm)$_{DTS-2b}$	2 SE
Whole rock	0.012	−7.5	1.5	−68	9	−139	18
Pyroxene	0.009	−7.1	2.7	−121	27	−260	63
Non-magnetic	6.02	−8.4	2.7	−294	15	−588	34

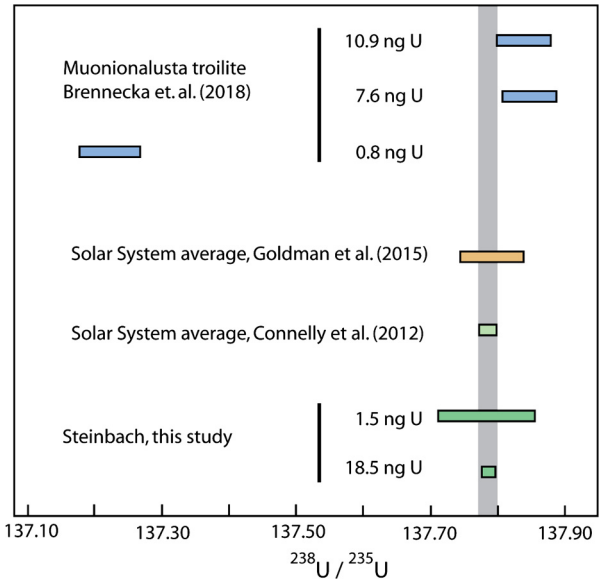

Fig. 4. The measured U isotopic composition of the Steinbach meteorite in comparison to estimates for the bulk Solar System and analyses of troilite samples from the paired IVA iron meteorite Muonionalusta.

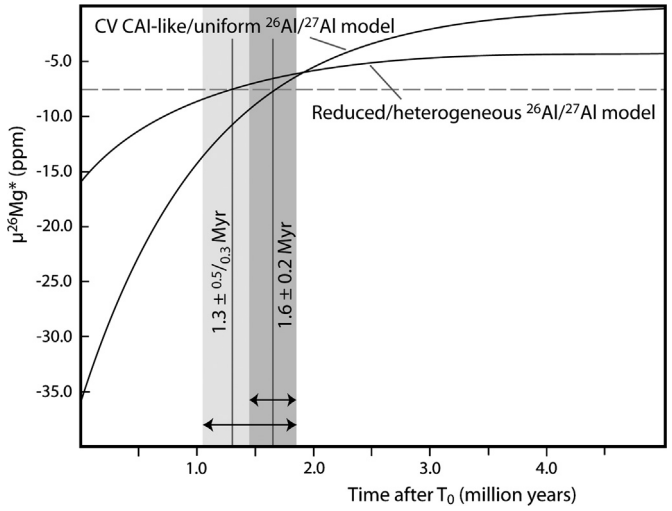

Fig. 5. Growth curves for μ^{26}Mg* on a body with a solar-like ^{27}Al/^{24}Mg ratio assuming: 1) a CV CAI-like initial ^{26}Al/^{27}Al ratio (5.2×10^{-5}) with a homogeneous distribution, and 2) a reduced ^{26}Al/^{27}Al ratio (1.6×10^{-5}) with a heterogeneous distribution after Larsen et al. (2011). The intersection of the curves and the initial μ^{26}Mg* value of −7.6 ppm for Steinbach define the timing of fractionation of this meteorite's parental magma for the respective ^{26}Al distribution models.

an appraisal of how to directly compare results using the different regression algorithms. These issues preclude the direct comparison of the Pb-Pb age of Muonionalusta reported by Blichert-Toft et al. (2010) with other ages as a robust estimate of the crystallization or cooling age of this meteorite.

The robustness of the age reported by Blichert-Toft et al. (2010) has also been questioned by Brennecka et al. (2018). Finding a wide range of U isotopic compositions for three fractions of Muonionalusta, they concluded that the U isotopic composition varies significantly between different troilite nodules rendering the age based on Pb-Pb data of Blichert-Toft et al. (2010) for a different nodule unsubstantiated. Brennecka et al. (2018) concluded that the Pb-Pb age of Blichert-Toft et al. (2010) may require a downward adjustment of up to 7 Myr considering their lowest determined ^{238}U/^{235}U ratio. However, we find a U isotopic composition for the IVA paired meteorite Steinbach that is indistinguishable from previous estimates for all meteoritic materials other than CAIs (Fig. 4; Connelly et al., 2012; Goldmann et al., 2015). As such, we suggest that it is more likely that the single anomalous U isotopic composition for one troilite reported by Brennecka et al. (2018) is an analytical artifact related to analyzing a small amount of U (0.79 ng) with a small interference on the minor ^{235}U isotope. This is supported by the fact that their other two troilite analyses of more U (10.9 ng and 7.7 ng) yielded corrected values that almost overlap with the Solar System value corroborated by Connelly et al. (2012) and Goldmann et al. (2015) (Fig. 4), as discussed by Brennecka et al. (2018). We conclude that there is no convincing evidence of any variations of U isotopic composition on the IVA parent body and that any discussion of significant degrees of U fractionation related to core formation is misguided by a single spurious analysis.

The whole rock, pyroxene and non-magnetic fractions yield overlapping μ^{26}Mg* values with a weighted average of -7.6 ± 1.2. The μ^{26}Mg* value of the mineral separate with a ^{27}Al/^{24}Mg value of 6.02 in a rock cooled by the Pb-Pb age of 1.83 ± 0.34 Myr after t_0 is predicted to have a μ^{26}Mg* value of >100 ppm assuming ingrowth from an initial μ^{26}Mg* value of −7.6 and an initial Solar System ^{26}Al/^{27}Al value after Larsen et al. (2011). That the measured value instead overlaps the low Al/Mg whole rock values (Fig. 3) requires that unradiogenic Mg from pyroxene surrounding the high Al/Mg phases has exchanged with the radiogenic Mg in the Mg-poor non-magnetic fraction, effectively erasing any signal of the predicted higher μ^{26}Mg*. This may have occurred during the protracted cooling after re-accretion of the parent body or during an unconstrained metamorphic event. Given that pyroxene preserves the radiogenic Pb isotopic composition corresponding to an age of 1.83 ± 0.34 Myr after t_0 requires that Pb did not diffuse in pyroxene at the temperatures capable of mobilizing Mg.

Regardless of the timing and mechanism of resetting of the high Al/Mg phase, the very low Al/Mg ratio of this sample means that radiogenic ^{26}Mg ingrowth since crystallization is negligible and the average μ^{26}Mg* of -7.6 ± 1.2 is effectively the initial value for Steinbach and, by extension, its source. Based on this initial μ^{26}Mg* value, a model age can be calculated for the timing of the fractionation that caused the low Al/Mg ratio in the source region. Assuming a Solar Al/Mg ratio of the precursor material of 0.1, an initial ^{26}Al/^{27}Al, solar initial μ^{26}Mg* value of −15.9 and a heterogeneous distribution of ^{26}Al/^{27}Al (all after Larsen et al., 2011) and no radiogenic ingrowth after cooling and closure of Steinbach, we calculate an age of $1.3^{+0.5}_{-0.3}$ Myr after CAI formation for this fractionation event (Fig. 5). Using the same model parameters except assigning the initial ^{26}Al/^{27}Al to that of CV CAIs (Jacobsen et al., 2008; Larsen et al., 2011) returns an age of 1.6 ± 0.2 Myr after CAI formation (Fig. 5). The two ages overlap within their respective uncertainties but we prefer to use the age based on the heterogeneous and reduced abundances of ^{26}Al in the inner Solar System as prescribed by Larsen et al. (2011) given the inner Solar System heritage of the Group IVA meteorites (Kruijer et al., 2017).

5.1. History of the Group IVA parent body

The reported large variations in cooling rates for the IVA meteorites (100 °C/yr to 6000 °C/Myr; Haack et al., 1996; Yang et al., 2007; Goldstein et al., 2014) in general and Steinbach specifically (see Ruzicka and Hutson (2006) for summary) are inconsistent with slow cooling rates predicted for a body with a fully mantled core. To account for these large variations, Yang et al. (2007) proposed a model in which a molten, differentiated parent body is disaggregated by an impact that was followed by re-accretion of the metallic core with a minor amount of silicate material. This model also accounts for the mixed metal-silicate composition of Steinbach and its association with the IVA iron meteorites. More specifically, the measured cooling rates of IVA iron meteorites can

be reproduced by a 300 ± 100 km diameter metallic core covered by ~1 km mantle of insulating silicate material (Yang et al., 2007, 2008). The relative proportions of mantle versus core are a post-impact feature that reflects the collision and re-accretion dynamics. Importantly, assuming a pre-impact chondritic starting composition suggests that the original body was ca. 1000 km in diameter prior to its disruption (Yang et al., 2007). This requires that the original accretion of planetary embryo, differentiation, disruption, reaccretion and cooling below the closure temperature of Pb in pyroxene all took place within 1.83 ± 0.34 Myr after CAI formation.

A cooling rate of 150 °C/Myr for Steinbach in the temperature range of 700-400 °C (Yang et al., 2007; Goldstein et al., 2014) is based on taenite lamellae in the metal. This relatively slow cooling rate over the temperature range for Pb retention in orthopyroxene places further constraints on the cooling history of IVA meteorites. The model Al-Mg age for Steinbach of $1.3^{+0.5}_{-0.3}$ Myr after CAI formation represents the timing of removal of Al-rich partial melts to form the low Al/Mg residue that would eventually become the source rocks for the silicate portion of Steinbach. This Al-Mg fractionation is inferred to have occurred prior to the impact-related breakup of the original parent body. Combined with the Pb-Pb age, these constraints leave a maximum interval of $0.53^{+0.60}_{-0.53}$Myr between impact and cooling at ~700 °C when the cooling rate is estimated to be 150 °C/Myr. This abbreviated timeframe for cooling requires initial cooling rates to have been much higher, in agreement with estimates of +100 °C/h for the low-Ca pyroxenes that crystallized early in Steinbach (Reid et al., 1974; Ulff-Møller et al., 1995; Haack et al., 1996). This transition from very high initial cooling rates to slower cooling over this short timeframe is most consistent with a shift from high heat loss while disaggregated immediately after impact to the slow cooling of a planetary embryo interior after re-accretion of mostly the metallic core, as suggested by Ruzicka and Hutson (2006).

5.2. Accretion models

In a long-standing paradigm, accretion of gas and dust to construct planets through oligarchical growth was an inefficient process that may have taken tens of millions of years to grow the planets within our Solar System (e.g. Tsiganis et al., 2005). There now exist multiple lines of convincing evidence from cosmochemistry and astronomy combined with numerical models from astrophysics to suggest a much more rapid time frame for planetary embryo accretion and differentiation. Just how fast this process actually occurred in the Solar System requires chronological constraints from appropriate samples capable of constraining the timing of assembly of planetary embryos. Our new age of 4565.47 ± 0.30 Ma for Steinbach dates the cooling of orthopyroxene through the closure temperature of Pb. As this phase formed as one of the last phases along the later slow cooling path, this part of this meteorite must have been fully crystalline by this time. The old age has important implications for the timing of accretion in general as it requires that accretion, differentiation, impact-driven disruption, re-accretion and the slow cooling at depth on the parent body all must have occurred by 1.83 ± 0.34 Ma after Solar System formation. This age is consistent with constraints from model Al-Mg silicate differentiation ages <1 Myr after CAI formation for achondrites (e.g. Schiller et al., 2011; Larsen et al., 2016; Van Kooten et al., 2016) and model Hf-W core formation ages for the major groups of iron meteorites of ca. 1 Myr after CAI formation that require accretion timescales of 0.1 to 0.3 Myr after CAI formation (e.g. Kruijer et al., 2014).

5.3. Implications for chondrule ages and ^{26}Al abundances in the solar protoplanetary disk

Combining models requiring chondrules for efficient planetary embryo formation (Johansen et al., 2015) with the implications of our old Pb-Pb for Steinbach, predicts that chondrules must have existed very early in the evolution of the protoplanetary disk. This is consistent with Pb-Pb chronometry and arguments based on the isotopic composition of initial Pb for chondrules that predict chondrules were created efficiently in the first 1 Myr and recycled for approximately 4 Myr when the protoplanetary disk was cleared. In contrast, assigning ages of chondrules using ^{26}Al-^{26}Mg chronometry predicts a paucity of chondrules during the first 1-2 Myr (Nagashima et al., 2018), a conclusion that is inconsistent with the efficient and early growth of planetary embryos by chondrule accretion.

The younger apparent ^{26}Al-^{26}Mg ages for chondrules are best explained by a reduced inventory of ^{26}Al relative to ^{27}Al in the protoplanetary disk, as suggested by Larsen et al. (2011) and Schiller et al. (2015). A reduced inventory of ^{26}Al adds an additional constraint on the timescales of accretion and differentiation assuming that the associated planetary melting is driven by ^{26}Al decay. As explored by Larsen et al. (2016) and Schiller et al. (2015), thermal models based on the reduced amount of ^{26}Al requires planetary accretion to be well underway by 0.15 Myr, a timeframe consistent with the Pb-Pb age of 1.83 ± 0.34 Ma after CAI formation for the Steinbach differentiated meteorite. As such, the Pb-Pb ages of chondrules and differentiated meteorites are best reconciled with the reduced ^{26}Al abundances in the protoplanetary disk and its impact on heating of planetary embryos and chronology based on this system.

5.4. Volatility and Pb loss in early Solar System processes

The low amount of initial Pb in either the orthopyroxene (0.75 ppb) or troilite (none detected) from Steinbach suggests that it was essentially absent in the precursor material to this meteorite before it crystallized. Given the solar abundances of Pb of 2.5 ppm predicted by analyses of CI chondrites (McDonough and Sun, 1995), the question arises as to the fate of Pb that was likely present in the precursor material. As Pb is a relatively volatile element with a $T_{50\%}$ condensation temperature of ca. 450 °C (Lodders, 2003), it is expected to have been lost by devolatization in any event where temperatures are elevated and diffusional length scales are appropriate. Models to explain the cooling history of IVA iron meteorites in general and Steinbach specifically envision an impact disruption of a molten or partially molten precursor planetary embryo. Such a scenario is expected to provide the temperatures and diffusional length scales necessary to efficiently loose Pb from this body, most plausibly after impact but before re-accretion during the debris disk phase. This is consistent with the reduced inventories of volatile major (S) and trace elements (Ga, Ge) that have also been ascribed to devolatization during the debris disk phase (Ruzicka and Hutson, 2006). The lack of initial Pb in Steinbach supports models of Pb loss by devolatization during the evolution of the angrite parent body (Connelly et al., 2008), the Moon-forming giant impact (Connelly and Bizzarro, 2016), the lunar magma ocean (Borg et al., 2011) and from chondrules during their (re)melting phase (Connelly et al., 2012 and Bollard et al., 2017). As such, there is a growing body of evidence supporting the efficient loss of Pb by devolatization during high temperature events, either through impacts, melting and/or convection during magma ocean evolution.

6. Conclusions

We report a U-corrected Pb-Pb age of 4565.47 ± 0.30 Ma for the Group IVA meteorite Steinbach, the oldest absolute age for an achondrite. A model ^{26}Al-^{26}Mg age based on fractions of the whole rock, pyroxene and non-magnetic minerals of $1.3^{+0.5}_{-0.3}$ Myr after CAI formation infers that the source material for this meteorite was depleted in Al by this time, most likely due to partial silicate melting and migration of the Al-rich partial melt to the surface of the planetary embryo. Thus, this model ^{26}Al-^{26}Mg age implies that the impact-related disruption of the IVA parent body did not occur before $1.3^{+0.5}_{-0.3}$ Myr after CAI formation. Combining these two ages with the large range of cooling rates from this group as a whole and Steinbach specifically requires that accretion of a >1000 km diameter planetary embryo, differentiation, impact disruption, re-accretion of the mainly metallic core and its cooling through 700 °C occurred by 1.83 ± 0.34 Myr after CAI formation. This supports a growing body of astronomical and cosmochemical evidence for the early, efficient growth of planetary embryos within the first million years of the Solar System's formation. The uniquely old age of Steinbach for an achondrite may reflect the accelerated cooling after primary accretion associated with the impact related disruption and re-accretion. Other parent bodies may have accreted as early as the original IVA parent body but will yield achondrites with younger ages due to their more normal, slower cooling histories. Accepting that chondrules are an essential ingredient for the rapid growth of the Group IVA original parent body requires that they were abundant in the formative stages of the protoplanetary disk. Conversely, a 1-2 Myr lag in the first formation of chondrules after CAI formation, as predicted by the ^{26}Al-^{26}Mg chronometer, is not compatible with this view. Instead, a reduced inventory of ^{26}Al early in the inner Solar System adequately explains the apparent gap and reconciles the chondrules age disparity between the ^{26}Al-^{26}Mg and Pb-Pb chronometers.

Acknowledgements

We thank Tsuyoshi Iizuka and an anonymous reviewer for their helpful comments. Funding for this project was provided by grants from the Danish Agency for Science, Technology and Innovation (J.N.C. - grant No. 12-125692), the Danish National Research Foundation (M.B. - grant No. DNRF97) and the European Research Council (M.B. - ERC Consolidator grant agreement 616027-STARDUST2ASTEROIDS).

References

Bizzarro, M., Paton, C., Larsen, K., Schiller, M., Trinquier, A., Ulfbeck, D., 2011. High-precision Mg-isotope measurements of terrestrial and extraterrestrial material by HR-MC-ICPMS – implications for the relative and absolute Mg-isotope composition of bulk silicate Earth. J. Anal. At. Spectrom. 26, 565–577.

Blackburn, T., Alexander, C.M.O'D., Carlson, R., Elkins-Tanton, L., 2017. The accretion and impact history of the ordinary chondrite parent bodies. Geochim. Cosmochim. Acta 200, 201–217.

Blichert-Toft, J., Moynier, F., Lee, C.-T.A., Telouk, P., Albaréde, F., 2010. The early formation of the IVA iron meteorite parent body. Earth Planet. Sci. Lett. 296, 469–480.

Bollard, J., Connelly, J.N., Whitehouse, M.J., Pringle, E.A., Bonal, L., Jørgensen, J.K., Nordlund, Å., Moynier, F., Bizzarro, M., 2017. Early formation of planetary building blocks inferred from Pb isotopic ages of chondrules. Sci. Adv. 3, e1700407.

Borg, L.E., Connelly, J.N., Boyet, M., Carlson, R.W., 2011. Chronological evidence that the Moon is either young or did not have a global magma ocean. Nature 477, 70–73.

Brennecka, G.A., Budde, G., Kleine, T., 2015. Uranium isotopic composition and absolute ages of Allende chondrules. Meteorit. Planet. Sci. 50, 1995–2002.

Brennecka, G.A., Amelin, Y., Kleine, T., 2018. Uranium isotope ratios of Muonionalusta troilite and complications for the absolute age of the IVA iron meteorite core. Earth Planet. Sci. Lett. 490, 1–10.

Condon, D.J., McLean, N., Noble, S.R., Bowring, S.A., 2010. Isotopic composition (^{238}U/^{235}U) of some commonly used uranium reference materials. Geochim. Cosmochim. Acta 74, 7127–7143.

Connelly, J.N., Bizzarro, M., Thrane, K., Baker, J.A., 2008. The Pb-Pb age of Angrite SAH99555 revisited. Geochim. Cosmochim. Acta 72, 4813–4824.

Connelly, J.N., Bizzarro, M., 2009. Pb–Pb dating of chondrules from CV chondrites by progressive dissolution. Chem. Geol. 259, 143–151.

Connelly, J.N., Bizzarro, M., Krot, A.N., Nordlund, Å., Wielandt, D., Ivanova, M.A., 2012. The absolute chronology and thermal processing of solids in the solar protoplanetary disk. Science 338, 651–655.

Connelly, J.N., Bizzarro, M., 2016. Lead isotope evidence for a young formation age of the Earth-Moon system. Earth Planet. Sci. Lett. 452, 36–43.

Connelly, J.N., Bollard, J., Bizzarro, M., 2017. Pb-Pb chronometry and the early Solar System. Geochim. Cosmochim. Acta 201, 345–363.

Gerstenberger, H., Haase, G., 1997. A highly effective emitter substance for mass spectrometric Pb isotope ratio determinations. Chem. Geol. 136, 309–312.

Goldmann, A., Brennecka, G., Noordmann, J., Weyer, S., Wadhwa, M., 2015. The uranium isotopic composition of the Earth and the Solar System. Geochim. Cosmochim. Acta 148, 145–158.

Goldstein, J.I., Yang, J., Scott, E.R.D., 2014. Determining cooling rates of iron and stony-iron meteorites from measurements of Ni and Co at kamacite-taenite interfaces. Geochim. Cosmochim. Acta 140, 297–320.

Haack, H., Scott, E.R.D., Rasmussen, K.L., 1996. Thermal and shock history of mesosiderites and their large parent asteroid. Geochim. Cosmochim. Acta 60, 2609–2619.

Jacobsen, B., Yin, Q.-Z., Moynier, F., Amelin, Y., Krot, A.N., Nagashima, K., Hutcheon, I.D., Palme, H., 2008. ^{26}Al/^{27}Al and ^{207}Pb/^{206}Pb systematics of Allende CAIs: canonical solar initial ^{26}Al/^{27}Al ratio reinstated. Earth Planet. Sci. Lett. 272, 353–364.

Johansen, A., Low, M.-M.M., Lacerda, P., Bizzarro, M., 2015. Growth of asteroids, planetary embryos, and Kuiper belt objects by chondrule accretion. Sci. Adv. 1, e1500109.

Kruijer, T.S., Fischer-Gödde, M., Kleine, T., Sprung, P., Leya, I., Wieler, R., 2013. Neutron capture on Pt isotopes in iron meteorites and the Hf-W chronology of core formation in planetesimals. Earth Planet. Sci. Lett. 361, 162–172.

Kruijer, T.S., Touboul, M., Fischer-Gödde, M., Bermingham, K.R., Walker, R.J., Kleine, T., 2014. Protracted core formation and rapid accretion of protoplanets. Science 344, 1150–1154.

Kruijer, T.S., Burkhardt, C., Budde, G., Kleine, T., 2017. Age of Jupiter inferred from the distinct genetics and formation times of meteorites. Proc. Natl. Acad. Sci. USA 114, 6712–6716.

Larsen, K.K., Trinquier, A., Paton, C., Schiller, M., Wielandt, D., Ivanova, M.A., Connelly, J.N., Nordlund, Å., Krot, A.N., Bizzarro, M., 2011. Evidence for magnesium isotope heterogeneity in the solar protoplanetary disk. Astrophys. J. Lett. 735, L37.

Larsen, K.K., Schiller, M., Bizzarro, M., 2016. Accretion timescales and style of asteroidal differentiation in an ^{26}Al-poor protoplanetary disk. Geochim. Cosmochim. Acta 176, 295–315.

Livermore, B.D., Connelly, J.N., Moynier, F., Bizzarro, M., 2018. Evaluating the robustness of a consensus ^{238}/U^{235}U value for U-Pb geochronology. Geochim. Cosmochim. Acta 237, 171–183.

Lodders, K., 2003. Solar System abundances and condensation temperatures of the elements. Astrophys. J. 591, 1220–1247.

Ludwig, K.R., 2003. Isoplot/Ex version 3.00, a geochronological toolkit for Microsoft Excel. Berkeley Geochronol. Center Spec. Publ. 4.

McDonough, W.F., Sun, S.-S., 1995. Composition of the Earth. Chem. Geol. 120, 223–253.

Nagashima, K., Kita, N.T., Luu, T.-H., 2018. ^{26}Al-^{27}Mg systematics of chondrules. In: Chondrules: Records of Protoplanetary Disk Processes. Cambridge University Press, pp. 247–275.

Paton, C., Hellstrom, J., Paul, B., Woodhead, J., Hergt, J., 2011. Iolite: freeware for the visualisation and processing of mass spectrometric data. J. Anal. At. Spectrom. 26, 2508–2518.

Reid, A.M., Williams, R.J., Takeda, H., 1974. Coexisting bronzite and clinobronzite and the thermal evolution of the Steinbach meteorite. Earth Planet. Sci. Lett. 22, 67–74.

Richter, S., Eykens, R., Kühn, H., Aregbe, Y., Verbruggen, A., Weyer, S., 2010. New average values for the ^{238}U/^{235}U isotope ratios of natural uranium standards. Int. J. Mass Spectrom. 295, 94–97.

Ruzicka, A., Hutson, M., 2006. Differentiation and evolution of the IVA meteorite parent body: clues from pyroxene geochemistry in the Steinbach stony-iron meteorite. Meteorit. Planet. Sci. 41, 1959–1987.

Schiller, M., Baker, J., Creech, J., Paton, C., Millet, M.A., Irving, A., Bizzarro, M., 2011. Rapid timescales for magma ocean crystallization on the howardite-eucrite-diogenite parent body. Astrophys. J. Lett. 740, L22.

Schiller, M., Connelly, J.N., Glad, A.C., Mikouchi, T., Bizzarro, M., 2015. Early accretion of protoplanets inferred from a reduced inner solar system ^{26}Al inventory. Earth Planet. Sci. Lett. 420, 45–54.

Schaudy, R., Wasson, J.T., Buchwald, V.F., 1972. The chemical classification of iron meteorites – VI. A reinvestigation of irons with Ge concentrations lower than 1 ppm. Icarus 17, 174–192.

Stacey, J.S., Kramers, J.D., 1975. Approximation of terrestrial lead isotope evolution by a two-stage model. Earth Planet. Sci. Lett. 26, 207–221.

Tsiganis, K., Gomes, R., Morbidelli, A., Levison, H.F., 2005. Origin of the orbital architecture of the giant planets of the Solar System. Nature 435, 459–461.
Ulff-Møller, F., Rasmussen, K.L., Kallemeyn, G.W., Prinz, M., Palme, E.H., Spettel, B., 1995. Differentiation of the IVA parent body: evidence from silicate-bearing iron meteorites. Geochim. Cosmochim. Acta 59, 4713–4728.
Van Kooten, E.M.M.E., Wielandt, D., Schiller, M., Nagashima, K., Thomen, A., Larsen, K.K., Olsen, M.B., Nordlund, Å., Krot, A.N., Bizzarro, M., 2016. Isotopic evidence for primordial molecular cloud material in metal-rich carbonaceous chondrites. Proc. Natl. Acad. Sci. USA 113, 2011–2016.
Yang, J., Goldstein, J.I., Scott, E.R.D., 2007. Iron meteorite evidence for early formation and catastrophic disruption of protoplanets. Nature 446, 888–891.
Yang, J., Goldstein, J.I., Scott, E.R.D., 2008. Metallographic cooling rates and origin of IVA iron meteorites. Geochim. Cosmochim. Acta 72, 3043–3061.